Particuology 22 (2015) 89–94

Contents lists available at ScienceDirect

Particuology

journal homepage: www.elsevier.com/locate/partic

Highly dispersed Mn_2O_3 microspheres: Facile solvothermal synthesis and their application as Li-ion battery anodes

Jianfei Yu[a], Lin Zhu[a,c], Cheng Fan[a], Cheng Zan[b], Ling Hu[a], Shuhui Yang[a], Qiang Zhang[a,*], Wancheng Zhu[c], Lin Shi[d], Fei Wei[a]

[a] Beijing Key Laboratory of Green Chemical Reaction Engineering and Technology, Department of Chemical Engineering, Tsinghua University, Beijing 100084, China
[b] State Key Laboratory of Enhanced Oil Recovery, Research Institute of Petroleum Exploration & Development, China National Petroleum Corporation, Beijing 100007, China
[c] Department of Chemical Engineering, Qufu Normal University, Shandong 273165, China
[d] Key Laboratory for Thermal Science and Power Engineering of Ministry of Education, Department of Thermal Engineering, Tsinghua University, Beijing 100084, China

ARTICLE INFO

Article history:
Received 21 August 2014
Received in revised form 5 October 2014
Accepted 11 October 2014

Keywords:
Mn_2O_3
Microspheres
Li-ion batteries
Solvothermal synthesis
Nanostructures

ABSTRACT

Nanostructured transition metal oxides are promising alternative anodes for lithium ion batteries. Li-ion storage performance is expected to improve if high packing density energy particles are available. Herein, Mn_2O_3 microspheres with a ca. 18 μm diameter and a tapped density of 1.33 g/cm^3 were synthesized by a facile solvothermal–thermal coversion route. Spherical $MnCO_3$ precursors were obtained through solvothermal treatment and they decomposed and converted into Mn_2O_3 microspheres at an annealing temperature of 700 °C. The Mn_2O_3 microspheres consisted of Mn_2O_3 nanoparticles with an average 40 nm diameter. These porous Mn_2O_3 microspheres allow good electrolyte penetration and provide an ion buffer reservoir to ensure a constant electrolyte supply. The Mn_2O_3 microspheres have reversible capacities of 590 and 320 mAh/g at 50 and 400 mA/g, respectively. We thus report an efficient route for the fabrication of energy particles for advanced energy storage.

1. Introduction

Rechargeable lithium ion batteries (LIBs) have become the dominant power source used in portable electronic devices because of their excellent low self-discharge rate, high coulombic energy efficiency, and the absence of a memory effect (Deng, Wan, Xie, Qin, & Chen, 2014; Su & Schlogl, 2010;). However, commercial LIB anode materials such as graphite have a relatively low Li storage capacity of only 372 mAh/g. Much effort has been put into the development of better electrode materials for LIBs to meet ever-growing performance demands (Cheng et al., 2013b; Gao et al., 2013; Jiang, Tang, Wu, Lin, & Qu, 2013; Zhang et al., 2014c).

Nanostructured transition metal oxides are the most widely investigated alternative anode materials for LIBs because of their large theoretical specific capacities (Yuan, Wu, Xie, & Lou, 2014). Among all transition metal oxides, manganese-based oxides have lower operating voltages (average discharge and charge voltages of 0.5 and 1.2 V, respectively). Anode materials with lower charge (battery discharge process) voltages versus Li/Li$^+$ can deliver a higher energy density. Manganese oxides (MnO_x) are an important class of the metal oxide family and are believed to be promising electrode materials because of their abundance, nontoxicity, and low cost. For instance, manganese oxides with excellent structural flexibility combined with unique chemical and physical properties are widely used in fields like heterogeneous catalysis (Han et al., 2008; Xu et al., 2012), electrocatalysis (Cheng et al., 2013a), supercapacitors (Xu, Kang, Li, & Du, 2010; Yan et al., 2010), and rechargeable batteries (Dai, Jiang, Hu, & Li, 2013; Wang et al., 2014; Zhang et al., 2014b). Among these, Mn_2O_3 possesses a high theoretical specific capacity (~1018 mAh/g) as an anode material for LIBs. Recently, Mn_2O_3 nanorods (Shen, Ji, Miao, Yang, & Chen, 2011), nanocubes (Wang et al., 2012), nanoplates (Zhang et al., 2014b), stacking nanoflowers (Zhang, Qian, Zhu, & Tang, 2014a), porous spheres (Chang et al., 2013; Deng et al., 2012;

* Corresponding author. Tel.: +86-10-62789041; fax: +86-10-62772051.
E-mail address: zhang-qiang@mails.tsinghua.edu.cn (Q. Zhang).

http://dx.doi.org/10.1016/j.partic.2014.10.007

Qiao, Yu, Jin, Guan, & Chen, 2014), nanochains (Salavati-Niasari, Mohandes, Davar, & Saberyan, 2009), nano-ovals (Qiu et al., 2011), and nanocones (Dai et al., 2013) have been reported. Both the structure and morphologies of Mn_2O_3 nanostructures can be easily tuned. However, their packing density is usually not very high and the volumetric density of the as-obtained electrodes should be further improved. An efficient method to fabricate high packing density Mn_2O_3 nanostructures with excellent Li-ion storage performance is thus required.

In this contribution, Mn_2O_3 microspheres were fabricated through the facile solvothermal synthesis from $MnCO_3$ precursors and subsequent calcination. Microspheres have a high tapped density and, therefore, are widely employed in the battery industry. The reason we selected solvothermal synthesis is because of advantages such as high efficiency, low cost, extraordinary homogeneity, ability to mix starting compounds on the molecular level, and flexibility to effectively tailor products by tuning synthetic parameters (Liu et al., 2012). As-obtained Mn_2O_3 microspheres exhibit good electrochemical performance as anode materials for LIBs.

2. Experimental

2.1. Synthesis of Mn_2O_3 microspheres

$Mn(NO_3)_2$, ethylene glycol ($C_2H_6O_2$, 99.9%), and HNO_3 (99.9%) were purchased from Beijing Chemical Company (China) and used as received. In the preparation of Mn_2O_3 microspheres, 2.0 mL 5.0 M $Mn(NO_3)_2$ and 2.0 mL 5.0 M HNO_3 solution were added to ethylene glycol. After stirring for 10 min, the mixtures were transferred to a 100 mL Teflon-lined vessel, which was sealed in an autoclave and then treated at 180 °C for 10.0 h. As the autoclave was cooled to room temperature naturally, the Mn_2O_3 precursors were collected from the reaction solution by centrifugation at 10,000 rpm for 10 min. The precursors were washed several times with ethanol and dried in air at 100 °C. The final Mn_2O_3 microspheres were obtained upon heat treatment of the precursors at 700 °C for 2.0 h in air.

2.2. Characterization

The as-prepared Mn_2O_3 microspheres were examined by X-ray diffraction (XRD, D8 Advance, Bruker, Germany; CuKα), scanning electron microscopy (SEM, JSF7401, JEOL, Japan; 3–20 kV), transmission electronic microscopy (TEM, JEOL2010, JEOL, Japan; 200 kV), Raman spectroscopy (Horiba JY, France; 633 nm laser), X-ray photoelectron spectroscopy (XPS, 250Xi, ESCALAB, USA; MgK_α), and thermogravimetric analysis (TGA, TGA/DSC1, Mettler Toledo, Switzerland; elevating heat rate: 10 °C/min, O_2 atmosphere).

2.3. Electrochemical measurements

The composite electrodes consisted of 80% Mn_2O_3, 10% carbon nanotubes (high purity, made by fluidized bed technology of Tsinghua University), and 10% polyvinylidene fluoride (PVDF, 761A, Arkema, France) by weight and were prepared by coating the mixture on copper foil. The 2025 coin cells use lithium foil as a counter electrode, a polypropylene microporous membrane as a separator and 1.0 M $LiPF_6$ dissolved in ethylene carbonate (EC), dimethyl carbonate (DMC), and ethylene methyl carbonate (EMC) (1:1:1, v/v/v) as the electrolyte. The cells were assembled in an argon-filled glove box. Charge–discharge measurements were carried out using a Neware battery testing system (CT3008 W) at 100 mA/g in the range of 0.01–3.0 V versus Li/Li^+.

3. Results and discussion

3.1. Structure of the Mn_2O_3 microspheres

$MnCO_3$ microspheres with a diameter of *ca.* 20 μm (Fig. 1(a)) were formed as precursors in the solvothermal process with $Mn(NO_3)_2$ and HNO_3 as oxidant, as well as ethylene glycol as the medium. Ethylene glycol provides abundant hydroxy ligands to coordinate with manganese ions, which reduces the hydrolysis rate of the manganese ions and induces the formation of spherical $MnCO_3$ precursor (Liang, Xu, Kuang, & Wang, 2008). The carboxyl groups produced by HNO_3 oxidation inhibit precursor hydrolysis and favor the formation of microspheres. The rough surfaces of the as-prepared $MnCO_3$ microspheres are composed of tiny grains. The spherical morphology of the $MnCO_3$ microspheres is attributed to energy minimization principle in these systems. After heat treatment under an air atmosphere at 700 °C for 2.0 h, the $MnCO_3$ microspheres decomposed into Mn_2O_3 microspheres. The Mn_2O_3 microspheres had an average diameter of about 18 μm. A tapped density of 1.33 g/cm^3 was obtained.

The crystal structures of the as-synthesized samples were determined by XRD (Fig. 1(c)). All the diffraction peaks of the precursor were indexed to rhombohedral $MnCO_3$ (JCPDS Card No. 85-1109, space group: R-3c, $a = b = 4.72926$ Å, $c = 15.48718$ Å, $\alpha = \beta = 90°$, $\gamma = 120°$) without other impurities. All the diffraction peaks of the precursors that were annealed at 700 °C were perfectly indexed to the cubic phase of Mn_2O_3 (JCPDS Card No. 24-0508, space group: Ia3, $a = b = c = 9.4091$ Å, $\alpha = \beta = \gamma = 90°$). According to the Scherrer formula, the as-obtained Mn_2O_3 had an average size of 40.6 nm. A high-resolution TEM image of Mn_2O_3 is shown in Fig. 1(d). The lattice fringe with an interplanar distance of 0.473 nm corresponds to the (200) plane of the cubic α-Mn_2O_3 structure.

To investigate the growth mechanism of the Mn_2O_3 microspheres, concentration-dependent shape evolution studies were also carried out. When using a 1.0 mL $Mn(NO_3)_2$ solution the $MnCO_3$ (Fig. S1) were found to be irregular grains because of Ostwald ripening. The thermal decomposition behavior of the $MnCO_3$ precursors was investigated by TGA and differential scanning calorimetric (DSC) methods (Fig. 2(a)). Three weight loss steps are present in the TGA profile. The first weight loss is between 30 and 250 °C in the TGA curve and comes from the desorption of physically absorbed water, glycol molecules, glycol oligomers, and other organic molecules (Chen, Yu, & Liang, 2011). The second sharp weight loss step between 250 and 400 °C corresponds to the decomposition and oxidation of chemically bonded organic species and the partial thermal decomposition of $MnCO_3$ to MnO in the precursors. The third weight loss step between 400 and 550 °C comes from the transformation of $MnCO_3$ and MnO to Mn_2O_3. In particular, 500 °C was found to be a critical temperature for the simultaneous decomposition of $MnCO_3$ and oxidation of MnO (Chang et al., 2013). The DSC curve exhibited an exothermic peak centered at about 260 °C and this corresponds well to the rapid weight loss in the TGA curve. Consequently, annealing the Mn_2O_3 precursors at 700 °C for 2.0 h induced the formation of pure α-Mn_2O_3. The specified surface area of the as-obtained α-Mn_2O_3 was 12.6 m^2/g and the pore volume was 0.018 cm^3/g (Fig. S2).

The Raman spectra of the Mn_2O_3 precursors and the samples annealed at 700 °C for 2.0 h are shown in Fig. 2(b). The Raman bands of around 200–1000 cm^{-1} come from the Mn—O vibration modes of manganese oxides. The Raman spectrum of the Mn_2O_3 precursors contains Mn—O vibrations of $MnCO_3$ and these are located at 953.1, 643.2, and 347.8 cm^{-1}. Three Raman bands are centered at 948.8, 628.6, and 335.5 cm^{-1} respectively, and these fit the Mn(III)—O modes observed in the reference Mn_2O_3 well (Han et al., 2008).

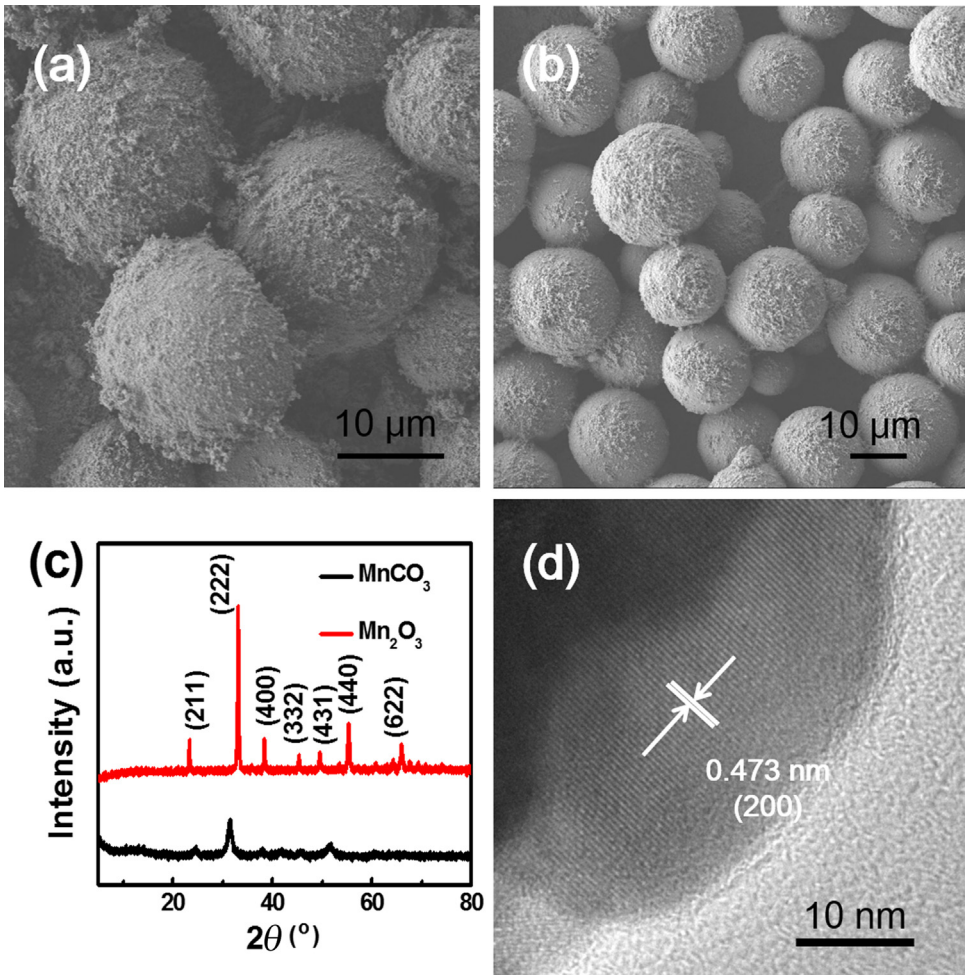

Fig. 1. Structure and morphology of the $MnCO_3$ precursor and the Mn_2O_3 microspheres: (a) SEM image of the $MnCO_3$ microsphere precursor produced by the solvothermal process; (b) SEM image of the Mn_2O_3 microspheres obtained by thermal decomposition of the $MnCO_3$ precursor annealed at 700 °C for 2.0 h; (c) XRD patterns; (d) HRTEM image.

An XPS measurement of the as-prepared Mn_2O_3 microspheres was carried out to identify the chemical state of Mn as well as the composition and purity of the samples (Fig. 2(c) and (d)). The binding energy (BE) values of Mn 2p1/2 and Mn 2p3/2 in the sample were 653.2 and 641.3 eV, respectively (Fig. 2(c)). Spin-orbit splitting was responsible for the difference between the BE values of the Mn 2p3/2 and Mn 2p1/2 levels. The observed spin-orbit splitting value was about 11.9 eV, which was nearly the same as that in manganese oxides. The BE of Mn 2p3/2 (641.3 eV) and spin-orbit splitting (11.9 eV) were nearly the same as the values reported for Mn_2O_3 (Salavati-Niasari et al., 2009). Oxygen spectra are also shown in Fig. 2(d). The O 1s peaks at 529.7 and 531.1 eV are attributed to oxygen O^{2-} in the lattice of Mn—O—Mn.

3.2. Mn_2O_3 microsphere formation mechanism

The formation of uniform Mn_2O_3 microspheres was investigated as follows. First, spherical $MnCO_3$ precursors were obtained through a soft-chemical process. Glycol acted as both a solvent and a ligand. Glycol was oxidized by HNO_3 and a series of organic ligands such as ethane diacid, ethanoic acid, and poly(ethylene glycol) formed. Manganese is oxyphilic and, therefore, it coordinates with these organic ligands to form hybrid precursors in the initial period. Because of the minimum surface energy principle, the precursors fabricated by the soft-chemical process have spherical morphology. During the annealing process, the noncrystalline precursors convert into the crystalline cubic phase of Mn_2O_3. The organic ligands decompose and combust leading to the maintenance of the microsphere's morphology (see Fig. 3).

3.3. Li-ion storage performance of Mn_2O_3 microspheres

The electrochemical performance of an as-prepared Mn_2O_3 microsphere electrode as an anode material for LIBs was investigated. Cyclic voltammetry (CV) profiles of the Mn_2O_3 microspheres are shown in Fig. 4(a). The voltammograms were measured at a sweeping rate of 0.1 mV/s in the potential range from 3.0 to 0.02 V vs. Li^+/Li at room temperature. The CV curve for the first cycle was different from that of subsequent cycles. The strong peak centered at 0.36 V in the first cathodic process was associated with the reduction of Mn^{2+} to Mn^0. In subsequent cycles the main cathodic peak shifted to about 0.30 V. For the anodic process, two peaks were present at 1.29 and 2.35 V, and these come from the oxidation of Mn^0 to Mn^{2+} and Mn^{2+} to Mn^{3+}, respectively. The first anodic peak shifted to 1.40 V because of the polarization induced by solid electrolyte formation during the first cycle. Compared with the first discharge process, the peak current decreased and this indicates capacity loss during the charging process. The cathodic peak for

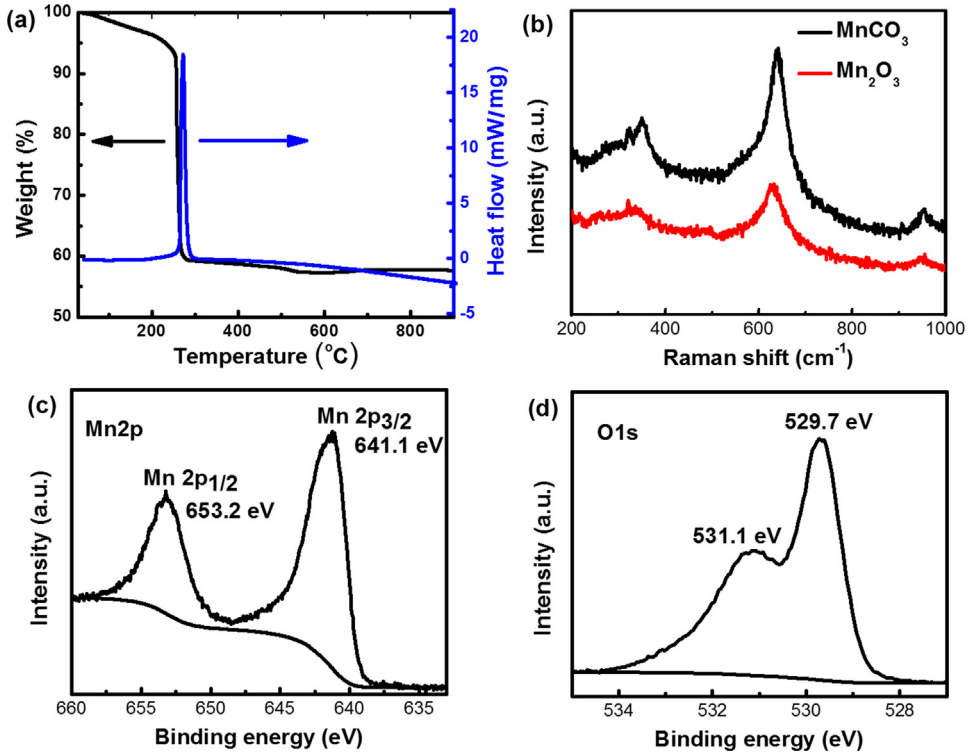

Fig. 2. Decomposition of the $MnCO_3$ precursors to Mn_2O_3 microspheres: (a) TGA and DSC profiles of the Mn_2O_3 precursors recorded from room temperature to 900 °C in air; (b) Raman spectra; (c) Mn 2p and, (d) O 1s XPS spectra of the as-prepared Mn_2O_3 microspheres.

Mn^{3+} to Mn^{2+} was faint. However, as shown in the discharge curves in Fig. 4(b), the slope at 1.5–0.4 V and the voltage plateau at 0.4 V come from Li-ion insertion for Mn^{3+} to Mn^{2+} and Mn^{2+} to Mn^0, respectively. The lithium storage mechanism of the Mn_2O_3 microspheres is as follows (Chang et al., 2013; Deng et al., 2012):

$$2Li^+ + 3Mn_2O_3 + 2e \rightarrow 2Mn_3O_4 + Li_2O \quad (1)$$

$$2Li^+ + Mn_3O_4 + 2e \rightarrow 3MnO + Li_2O \quad (2)$$

$$MnO + 2Li^+ + 2e \rightarrow 4Li_2O + Mn \quad (3)$$

With an increase in current density the discharge capacity of the Mn_2O_3 anode decreases gradually. Specific discharge capacities of 590, 435, 377, and 320 mAh/g at 50, 100, 200, and 400 mA/g, respectively, were obtained (Fig. 4(c)). This is similar to the Li-ion storage performance reported for porous Mn_2O_3 spheres (~300 mAh/g at 200 mA/g for Mn_2O_3 calcined at 700 °C) (Chang et al., 2013), straw-sheaf-shaped Mn_2O_3 (~370 mAh/g at 400 mA/g) (Qiu et al., 2011), and hollow Mn_2O_3 nanocones (380 mAh/g at 400 mA/g) (Dai et al., 2013). This good rate performance is attributed to rapid ion diffusion through the mesopores of the Mn_2O_3 microspheres.

The cycling stability of the Mn_2O_3 microspheres was evaluated at a current density of 100 mAh/g. Fig. 4(d) shows plots of the discharge capacity and coulombic efficiency versus cycle number. A rapid capacity fading was detected over the initial five cycles, and this stabilized over the following 95 cycles. The coulombic efficiency was nearly 100% for the whole test. These results indicate that the Mn_2O_3 microspheres possess impressive Li-ion storage performance, which is better than that of reported pure porous Mn_2O_3 spheres (Chang et al., 2013) and also superior to nanocarbon anodes (Cheng et al., 2013b).

The good Li-ion storage performance of Mn_2O_3 microspheres can be attributed to the following aspects. First, the porous Mn_2O_3 microspheres allow good electrolyte penetration and an ion buffer reservoir to ensure a constant supply of electrolyte, even at high rates. Second, microspheres are ideal structures to accommodate the stress induced by volume changes during cycling, and the close packing of microspheres results in an anode with a high volumetric density. Li-ion storage performance can be further improved using a combination of nanocarbon structures as short-range current collectors from nanosized Mn_2O_3 nanoparticles.

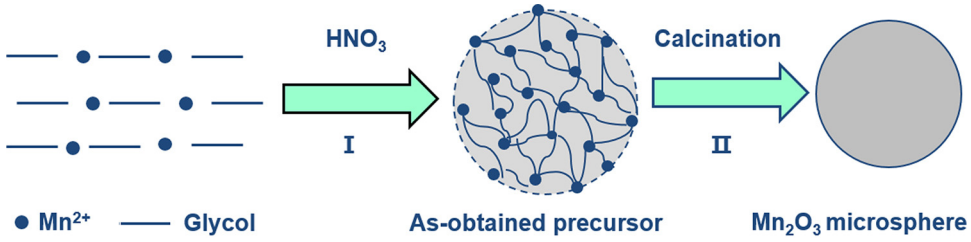

Fig. 3. Proposed formation mechanism for the Mn_2O_3 microspheres.

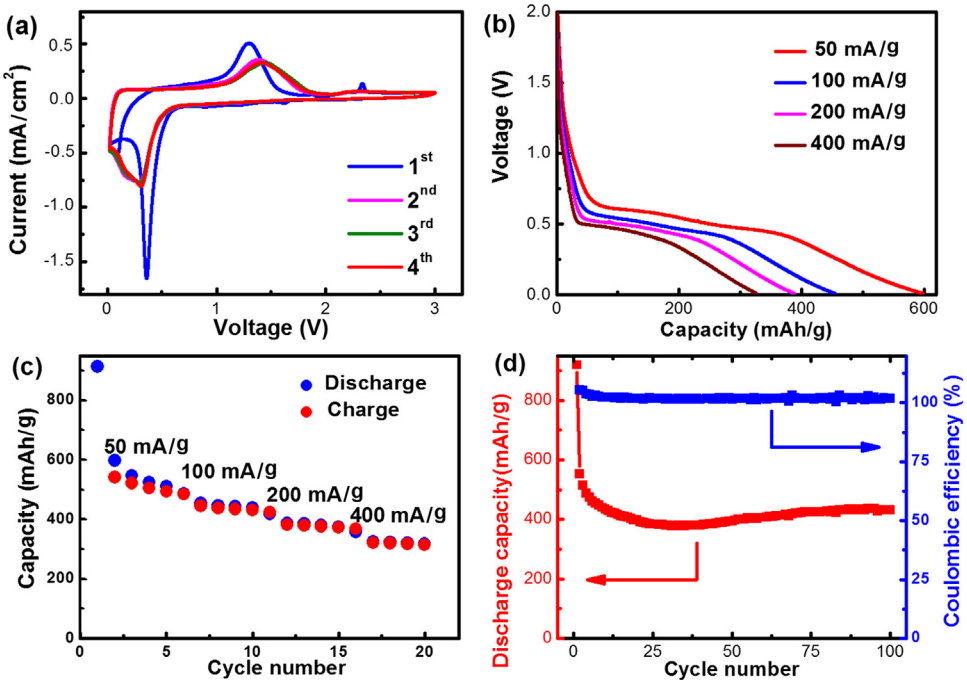

Fig. 4. (a) The CVs of the Mn_2O_3 electrode from 0.02–3.0 V versus Li^+/Li at a scan rate of 0.10 mV/s; (b) discharge curves and (c) rate performance at different current densities from 50–400 mA/g; (d) long-life cycling performance at 0.10 C (1.0 C = 1018 mAh/g).

4. Conclusions

Mn_2O_3 microspheres of *ca.* 18 μm in size were synthesized by a general, facile solvothermal–thermal coversion route. The porous Mn_2O_3 microspheres allow good electrolyte penetration and an ion buffer reservoir to ensure a constant supply of electrolyte. They exhibit a reversible capacity of 590 and 320 mAh/g at 50 and 400 mA/g, respectively. Microspheres with a packing density of 1.33 g/cm^3 are ideal structures to accommodate the stress. Mn_2O_3 microspheres have potential application as anodes in lithium ion batteries with high energy density. This work offers a facile method to fabricate advanced functional particles for energy storage.

Acknowledgments

This work was supported by the National Natural Science Foundation of China (21422604), the PetroChina Technology R&D Project on New Technology and the Method for Oil & Gas Development (2011A-1006), and CNPC Innovation Foundation (2014D-5006-0207).

Appendix A. Supplementary data

Supplementary material related to this article can be found, in the online version, at http://dx.doi.org/10.1016/j.partic.2014.10.007.

References

Chang, L., Mai, L. Q., Xu, X., An, Q. Y., Zhao, Y. L., Wang, D. D., et al. (2013). Pore-controlled synthesis of Mn_2O_3 microspheres for ultralong-life lithium storage electrode. *RSC Advances*, *3*, 1947–1952.

Chen, B. H., Yu, J. F., & Liang, X. (2011). $LaAlO_3$ hollow spheres: Synthesis and luminescence properties. *Langmuir*, *27*, 11654–11659.

Cheng, F. Y., Zhang, T. R., Zhang, Y., Du, J., Han, X. P., & Chen, J. (2013). Enhancing electrocatalytic oxygen reduction on MnO_2 with vacancies. *Angewandte Chemie—International Edition*, *52*, 2474–2477.

Cheng, X. B., Tian, G. L., Liu, X. F., Nie, J. Q., Zhao, M. Q., Huang, J. Q., et al. (2013). Robust growth of herringbone carbon nanofibers on layered double hydroxide derived catalysts and their applications as anodes for Li-ion batteries. *Carbon*, *62*, 393–404.

Dai, Y. H., Jiang, H., Hu, Y. J., & Li, C. Z. (2013). Hydrothermal synthesis of hollow Mn_2O_3 nanocones as anode material for Li-ion batteries. *RSC Advances*, *3*, 19778–19781.

Deng, Y., Wan, L., Xie, Y., Qin, X., & Chen, G. (2014). Recent advances in Mn-based oxides as anode materials for lithium ion batteries. *RSC Advances*, *4*, 23914–23935.

Deng, Y. F., Li, Z. N., Shi, Z. C., Xu, H., Peng, F., & Chen, G. H. (2012). Porous Mn_2O_3 microsphere as a superior anode material for lithium ion batteries. *RSC Advances*, *2*, 4645–4647.

Gao, G., Zhang, Q., Wang, K., Song, H., Qiu, P., & Cui, D. (2013). Axial compressive α-Fe_2O_3 microdisks prepared from CSS template for potential anode materials of lithium ion batteries. *Nano Energy*, *2*, 1010–1018.

Han, Y. F., Chen, L., Ramesh, K., Widjaja, E., Chilukoti, S., Surjami, I. K., et al. (2008). Kinetic and spectroscopic study of methane combustion over α-Mn_2O_3 nanocrystal catalysts. *Journal of Catalysis*, *253*, 261–268.

Jiang, J. J., Tang, X. L., Wu, R., Lin, H. Q., & Qu, M. Z. (2013). Electrochemical performance of polygonized carbon nanofibers as anode materials for lithium-ion batteries. *Particuology*, *11*, 401–408.

Liang, X., Xu, B. A., Kuang, S. M., & Wang, X. (2008). Multi-functionalized inorganic–organic rare earth hybrid microcapsules. *Advanced Materials*, *20*, 3739–3744.

Liu, X. F., Huang, J. Q., Zhang, Q., Liu, X. Y., Peng, H. J., Zhu, W. C., et al. (2012). N-methyl-2-pyrrolidone-assisted solvothermal synthesis of nanosize orthorhombic lithium iron phosphate with improved Li-storage performance. *Journal of Materials Chemistry*, *22*, 18908–18914.

Qiao, Y., Yu, Y., Jin, Y., Guan, Y. B., & Chen, C. H. (2014). Synthesis and electrochemical properties of porous double-shelled Mn_2O_3 hollow microspheres as a superior anode material for lithium ion batteries. *Electrochimica Acta*, *132*, 323–331.

Qiu, Y. C., Xu, G. L., Yan, K. Y., Sun, H., Xiao, J. W., Yang, S. H., et al. (2011). Morphology-conserved transformation: Synthesis of hierarchical mesoporous nanostructures of Mn_2O_3 and the nanostructural effects on li-ion insertion/deinsertion properties. *Journal of Materials Chemistry*, *21*, 6346–6353.

Salavati-Niasari, M., Mohandes, F., Davar, F., & Saberyan, K. (2009). Fabrication of chain-like Mn_2O_3 nanostructures via thermal decomposition of manganese phthalate coordination polymers. *Applied Surface Science*, *256*, 1476–1480.

Shen, X. P., Ji, Z. Y., Miao, H. J., Yang, J. A., & Chen, K. M. (2011). Hydrothermal synthesis of $MnCO_3$ nanorods and their thermal transformation into Mn_2O_3 and Mn_3O_4 nanorods with single crystalline structure. *Journal of Alloys and Compounds*, *509*, 5672–5676.

Su, D. S., & Schlogl, R. (2010). Nanostructured carbon and carbon nanocomposites for electrochemical energy storage applications. *ChemSusChem*, *3*, 136–168.

Wang, J. F., Zhu, G., Deng, L. J., Kang, L. P., Hao, Z. P., & Liu, Z. H. (2012). Novel synthesis and formation process of uniform Mn_2O_3 cubes. *CrystEngComm*, *14*, 8253–8260.

Wang, X. Z., Qiu, S., Lu, G. X., He, C. Z., Liu, J. R., Luan, L. Q., et al. (2014). Fabrication of porous MnO microspheres with carbon coating for lithium ion battery application. *CrystEngComm*, *16*, 1802–1809.

Xu, C. J., Kang, F. Y., Li, B. H., & Du, H. D. (2010). Recent progress on manganese dioxide based supercapacitors. *Journal of Materials Research*, *25*, 1421–1432.

Xu, J., Ouyang, L. K., Luo, Y., Xu, X. M., Yang, Z., Zhang, C. X., et al. (2012). Mechanistic insights into methanol-to-olefin reaction on an α-Mn_2O_3 nanocrystal catalyst. *AIChE Journal*, *58*, 3474–3481.

Yan, J., Fan, Z. J., Wei, T., Qian, W. Z., Zhang, M. L., & Wei, F. (2010). Fast and reversible surface redox reaction of graphene—MnO_2 composites as supercapacitor electrodes. *Carbon*, *48*, 3825–3833.

Yuan, C. Z., Wu, H. B., Xie, Y., & Lou, X. W. (2014). Mixed transition-metal oxides: Design, synthesis, and energy-related applications. *Angewandte Chemie—International Edition*, *53*, 1488–1504.

Zhang, X., Qian, Y. T., Zhu, Y. C., & Tang, K. B. (2014). Synthesis of Mn_2O_3 nanomaterials with controllable porosity and thickness for enhanced lithium-ion batteries performance. *Nanoscale*, *6*, 1725–1731.

Zhang, Y. J., Yan, Y., Wang, X. Y., Li, G., Deng, D. R., Jiang, L., et al. (2014). Facile synthesis of porous Mn_2O_3 nanoplates and their electrochemical behavior as anode materials for lithium ion batteries. *Chemistry—A European Journal*, *20*, 6126–6130.

Zhang, Z. L., Wang, Y. H., Ren, W. F., Tan, Q. Q., Chen, Y. F., Li, H., et al. (2014). Scalable synthesis of interconnected porous silicon/carbon composites by the rochow reaction as high-performance anodes of lithium ion batteries. *Angewandte Chemie—International Edition*, *53*, 5165–5169.